DOI: 10.1002/ejic.200600252

Tricarbonylchlororhenium(I) Carboxaldimine Derivatives: Synthesis, Structure, and NMR Characterization of *Z* and *E* Isomers

Claudio Garino,[a] Simona Ghiani,[a] Roberto Gobetto,[a] Carlo Nervi,*[a] Luca Salassa,[a] Gianluca Croce,[b] Marco Milanesio,[b] Edward Rosenberg,*[c] and J. B. Alexander Ross[c]

Keywords: *E*/*Z* isomerization / Density functional calculations / N ligands / Rhenium

The ligand *N*-(2-pyridylmethyl)anthracene-9-carboxaldimine (**1**) has been synthesized and characterized by NMR spectroscopic techniques. The experimental procedure leads selectively to the *E* isomer, which has been studied by a combined theoretical (Density Functional Theory) and 2D NOESY NMR spectroscopic approach. The trifluoroacetic acid promotes the *E* to Z isomerization of **1**. The process has been investigated by NMR spectroscopy and computationally for the neutral ligand **1**. DFT methods calculate that the *E* isomer is 2.2 kcal/mol more stable than the *Z* isomer, whereas the reverse situation is observed for the protonated species, where the *Z* isomer is 4.5 kcal/mol more stable than the *E* isomer. Transition state calculations for the interconversion of the neutral and protonated *E* species into their corresponding *Z* isomers show that the energy barriers are 27.6 and 20.3 kcal/mol for the neutral and protonated species, respectively. The reaction with pentacarbonylchlororhenium leads, in the absence and in the presence of trifluoroacetic acid, to the synthesis of the corresponding tricarbonylchlororhenium isomer complexes **Re-*E*-1** and **Re-*Z*-1**, respectively. Compounds **Re-*E*-1** and **Re-*Z*-1** were characterized by 1D and 2D NMR spectroscopy in solution, and their crystal structures were determined. Their photophysical and electrochemical properties are also reported.

Introduction

The electrochemical, photophysical, and photochemical properties of α,α′-diimino ligands have made their coordination chemistry with transition metals, in particular with ruthenium, one of the most relevant in recent decades.[1–4] $Re(CO)_3X$ (where X = halogen) derivatives bearing α,α′-diimine ligands have been studied for their effectiveness in the electrocatalytic reduction of CO_2[5,6] and for their photo-induced electron and energy transfer properties.[7,8] The nitrogen atoms contained in these ligands are most commonly part of heterocyclic rings like pyridine, pyrimidine, and pyrazine. In comparison, less attention has been devoted to the investigation of similar Schiff base ligands, such as carboxaldimines, in which at least one nitrogen atom is not part of an aromatic ring. Rhenium derivatives with 2,2′-azobispyridine,[9–11] pyridinylmethylene amino derivatives,[8,12] and the $Re(CO)_3$ mediated Schiff base formation from the in situ reaction between pyridinecarbaldehyde and NH_2-containing biomolecules[13] have been studied. This class of compounds is of great interest because of their close relationship with their better-known counterparts, mentioned above. Furthermore, the imine functional group has become important in the synthesis of therapeutic agents, for example the third generation of the class of antibiotics known as cephalosporins,[14] and in the modeling of metal biosites in proteins and enzymes.[15] They have also attracted interest in asymmetric homogeneous and heterogeneous catalysis,[16] and in the synthesis of chiral heterocycles.[17] Their photophysical properties have also been studied theoretically by means of DFT calculations.[18,19] Because of the lower energy of the π* states, in metal complexes containing Schiff base ligands, their adsorption and emission MLCT bands show a red shift when compared with the MLCT transitions of the corresponding bipyridyl derivatives. This red shift can be explained in terms of a distortion of the excited states (π-π* and n-π*) that are localized on the C=N double bond and that contribute significantly to the composition of the LUMO,[20–22] especially in the case of carboxaldimines.[12] In general, imine–metal complexes are relatively unstable towards hydrolysis, particularly in the case of ruthenium and osmium.[23] Bulky ligands could be employed in the synthesis of more stable metal complexes with the aim of limiting or blocking such hydrolysis. Also, the acid-catalyzed *E*/*Z* isomerization is well known and several attempts towards understanding its mechanism have been made.[14] Yet, in some cases the de-

[a] Dipartimento di Chimica IFM, Università di Torino, via P. Giuria 7, 10125, Torino, Italy
Fax: +39-011-6707855
E-mail: carlo.nervi@unito.it
[b] Dipartimento di Scienze e Tecnologie Avanzate, Università del Piemonte Orientale "A. Avogadro", via Bellini 25/G, 15100 Alessandria, Italy
[c] Department of Chemistry, University of Montana, Missoula, MT 59812, USA
Supporting information for this article is available on the WWW under http://www.eurjic.org or from the author.

tails of the isomerization mechanism itself remain unclear. In this contribution we report the coordination of tricarbonylchlororhenium to the new organic ligand *N*-(2-pyridylmethyl)anthracene-9-carboxaldimine (**1**) in its *Z* and *E* isomeric forms, which leads to the synthesis of rather stable complexes.

Results and Discussion

Z and *E* Isomers of the Ligand 1

The ligand *N*-(2-pyridylmethyl)anthracene-9-carboxaldimine (**1**), was synthesized in refluxing ethanol by the condensation of 2-(aminomethyl)pyridine with anthracene-9-carboxaldehyde (Scheme 1).

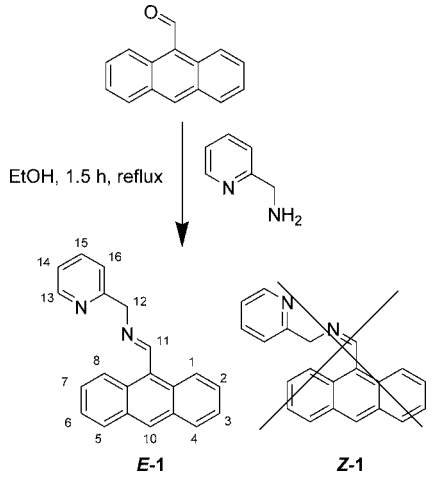

Scheme 1.

The imine **1** can exist in the *E* or *Z* isomeric forms. The presence/absence of bulky groups is generally accepted as the main reason for the preferential formation of one isomer over the other. However, to the best of our knowledge, a complete understanding of the process is not available to date. It is interesting to note that the procedure shown in Scheme 1 yields the isomer ***E*-1**, exclusively (see below). In the DFT-optimized structures of *E* and *Z* isomers, obtained using Jaguar[24] at the B3LYP/6-311++G** level, the two planes defined by the C=N imine and the anthracene moieties are perpendicular to each other. This situation is commonly found whenever an imine carries bulky groups.[25,26] From the DFT calculations it turns out that these geometries have a plane of symmetry, and that the *Z* isomer is only 0.8 kcal/mol more stable than the *E* form. The difference in energy is very small and much lower than the expected accuracy of the DFT method (about 2 kcal/mol).[27] The DFT calculations were repeated by using Gaussian 03[28] for the conformations resulting from 10° rotations around the imine bond. The highest energy conformation was noted at 90°, and the calculated value of 53 kcal/mol for the C=N rotational barrier appears to be fairly high. A similar value (56 kcal/mol) has been obtained for the rotational pathway of the *E*/*Z* isomerization in methyleneimine.[29] Attempts to gain thermal corrections based on harmonic frequencies from these symmetric structures of ***E*-1** and ***Z*-1** failed because of the oscillations of the computed energies. The difficulty in getting stable frequency calculations, and the fact that we get more than one imaginary frequency, suggested that these symmetric forms are only at a local rather than a global energy minimum (saddle point). In order to overcome these local minima of energies, we started from slightly distorted structures and excluded the use of symmetry during the optimization process. The geometries of *E* and *Z* isomers corresponding to the global minima, found by DFT optimizations with Jaguar at the same level, namely B3LYP/6-311++G**, are shown in Figure 1. The frequency calculations performed on these optimized asymmetric structures reveal that the *E* form is more stable than the *Z* form by 2.2 kcal/mol. Thus, better thermodynamic agreement with the experimental observations is obtained, although the difference in energy is still comparable with the accuracy of the DFT method. The calculated structures of *E* and *Z* have very different intramolecular H–H distances (see Table 1), which are doubled in the case of the asymmetric ones because the two geminal H(12) and the two H(1) and H(8) hydrogen atoms are not equivalent. However, whatever the real dynamic structures are, both the symmetrical (local minimum) and nonsymmetrical (global minimum) structures of *Z* have H(11)–H(12) distances that are larger than those of the *E* isomers. This peculiarity is revealed experimentally by the phase-sensitive NOESY spectrum, in which an evident cross-peak system from the dipolar interaction between the lone H(11) and the two H(12) hydrogen atoms is clear evidence of the presence of the ***E*-1** isomer. Proton NMR resonances have been assigned by conventional 1D, 2D COSY, and NOESY spectra (see Supporting Information), and are summarized in Table 2. Moreover, variable temperature experiments performed on ***E*-1** in the range 220–300 K do not produce any changes in the NMR spectra, revealing that *Z* and *E* isomers are not easily interconverted. Having obtained both the optimized structures, we have performed a search for the transition state (TS) associated with the isomerization of neutral ***E*-1** to ***Z*-1**. The optimized TS structure is provided in Figure 2 (a). The calculated structure of the TS shows that the bond angle C=N–C is linear, clearly indicating that the isomerization of the neutral species proceeds via an in-plane lateral shift process. The calculated free energy of the TS relative to the reactant, i.e. the energetic barrier for isomerization of neutral ***E*-1** to ***Z*-1** is moderately high (27.6 kcal/mol), but much lower than the energetic barrier associated with the pure C=N rotation. Similar values were calculated for the in-plane lateral shift process of methyleneimine (32.5 kcal/mol) and dicyandiamide (29 kcal/mol).[29,30]

However, when a slight molar excess of CF_3COOH is added to a CD_2Cl_2 solution of ***E*-1**, the resonances of H(11) and H(12) shift from 9.63 and 5.23 to 10.34 and 5.94 ppm, and then rapidly convert into two new resonances at 11.40 and 4.80 ppm, respectively. The conversion does not occur significantly when only a catalytic amount of acid is used, at least not over short periods. This new species does not

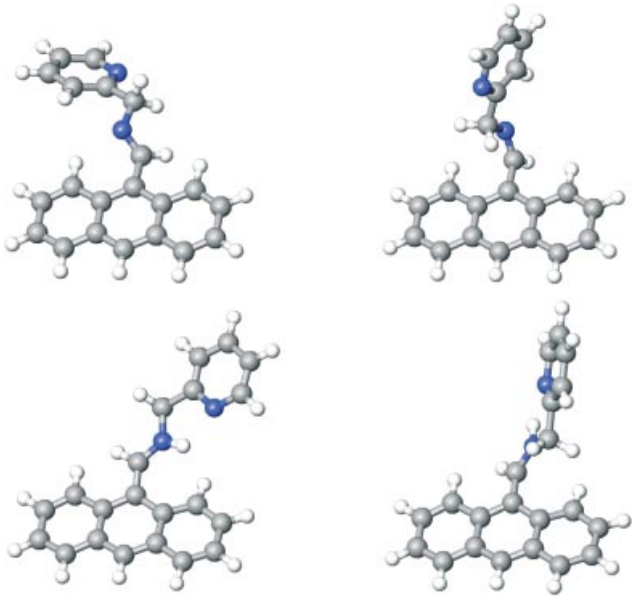

Figure 1. DFT optimized geometries of the ligand **1**. Neutral (up) and protonated (down) forms, and isomers *E* (left) and *Z* (right), at the B3LYP/6-311G++** level.

Table 1. Selected H–H distances [Å] of the optimized DFT geometries for the two isomers of **1** (local minimums, C_s symmetry, and global minimums, no symmetry).

Distances	*Z*	*E*	*Z* asymmetric	*E* asymmetric
H(11)–H(12)	3.686	2.558	3.645	3.136
			3.848	2.166
H(11)–H(1),H(8)	2.855	2.893	2.557, 3.133	2.065, 3.579
H(12)–H(1),H(8)	2.958	3.343	3.727, 3.334	4.232, 4.172
			4.879, 2.537	3.767, 4.047

Table 2. Experimental and calculated ^{1}H NMR resonances for ***E*-1** and ***Z*-1**.

H	Experimental		Symmetric, calculated by Gaussian 03 Asymmetric, calculated by Jaguar 6.5 (mean)	
	***E*-1**	**[*Z*-1H]$^+$**	***E*-1**	***Z*-1**
1	8.61	9.02	8.22	8.44
			9.82 (9.31)	8.25 (8.33)
8	8.61	9.02	8.22	8.44
			8.80 (9.31)	8.40 (8.33)
2	7.52	7.75	7.61	7.84
			7.81 (7.86)	7.89 (7.82)
7	7.52	7.75	7.61	7.84
			7.91 (7.86)	7.76 (7.82)
3	7.52	7.60	7.65	7.82
			7.75 (7.78)	7.83 (7.79)
6	7.52	7.60	7.65	7.82
			7.81 (7.78)	7.76 (7.79)
4	8.06	8.12	8.31	8.31
			8.30 (8.33)	8.42 (8.40)
5	8.06	8.12	8.31	8.31
			8.37 (8.33)	8.38 (8.40)
10	8.53	8.82	8.90	8.70
			8.83	8.86
11	9.63	11.40	10.18	9.74
			10.27	9.94
12	5.23	4.80	5.51	4.53
			6.01, 5.12 (5.56)	4.98, 4.44 (4.71)
13	8.59	8.80	8.99	9.04
			8.94	8.66
14	7.23	8.58 or 8.06	7.27	7.21
			7.33	7.08
15	7.72	8.06 or 8.58	7.73	7.54
			8.00	7.86
16	7.52	8.19	7.35	6.55
			8.59	8.39

show the above-mentioned NOESY cross peak signal (see Supporting Information). The overall process is therefore explained as (a) instantaneous protonation of ***E*-1**, (***E*-1H$^+$**) and (b) relatively fast conversion into the protonated ***Z*-1** form (***Z*-1H$^+$**). Thus ***E*-1** is easily converted into ***Z*-1** by adding trifluoroacetic acid. The trend in the proton resonance sequences on going from ***E*-1** to ***E*-1H$^+$**, and finally to the ***Z*-1H$^+$** form is more difficult to interpret. As mentioned, for H(11) and H(12) the experimental sequences are 9.63 to 10.34 to 11.40 ppm and 5.23 to 5.94 to 4.80 ppm, respectively. We optimized the geometries of ***E*-1**, ***E*-1H$^+$** and ***Z*-1H$^+$**, and the corresponding calculated ^{1}H NMR chemical shift sequences of H(11) and H(12) are 10.18 to 10.45 to 10.51 ppm and 5.51 to 5.59 to 4.81 ppm, respectively. Although quantum mechanical calculations of ^{1}H NMR chemical shifts are subject to significant errors,[31–33] especially whenever hydrogen bonds are involved, the same experimental trend is reproduced. More importantly, a frequency calculation gives a Gibbs free energy value for ***Z*-1H$^+$** that is 4.5 kcal/mol lower than that of the corresponding ***E*-1H$^+$**. This small but significant inversion of energy gives further support to the outlined interpretation, and it is in agreement with the experimental observation, which

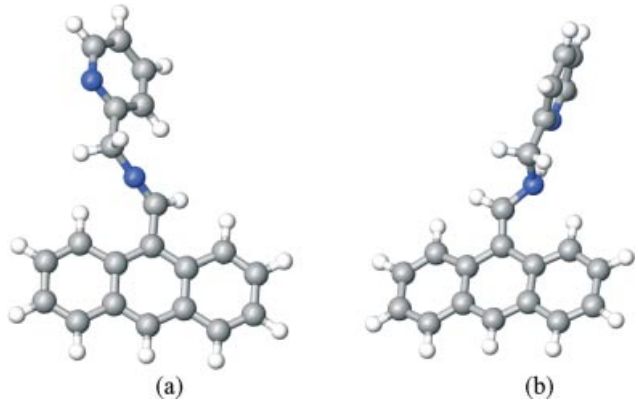

Figure 2. Transition State (TS) optimized structures for the isomerization processes ***E*-1** to ***Z*-1** (a) and ***E*-1H$^+$** to ***Z*-1H$^+$** (b).

shows that the ratio between the integrated ^{1}H NMR resonances H(12) of ***E*-1H$^+$** and ***Z*-1H$^+$**, namely the signals centered at δ = 5.94 and 4.80 ppm, respectively, are 1:16 (see Supporting Information). This corresponds to a Gibbs free energy difference of 1.6 kcal/mol between the two isomers at 298 K, in reasonable agreement with the calculated value. Computational searches for the TS for the isomerization process ***E*-1H$^+$** to ***Z*-1H$^+$** leads to the structure shown in

Figure 2 (b). The calculated free energy of the TS relative to the reactant ***E*-1H$^+$** is evaluated to be 20.3 kcal/mol. As one could expect, in both the neutral and protonated TSs, the dihedral angle that defines the rotation around the C=N double bond, $D_{C=N}$, is roughly midway between the values observed for the *Z* and *E* isomers. However, it is interesting to note that the protonated TS has a $D_{C=N}$ value closer to that of the *Z* isomer. The $D_{C=N}$ values for ***E*-1H$^+$**, ***Z*-1H$^+$**, and for the corresponding TS are 178.3, 12.0, and 111.5°, respectively, whereas the $D_{C=N}$ values for ***E*-1**, ***Z*-1**, and for the corresponding neutral TS are 179.3, 0.8, and 89.4°, respectively. The neutral and protonated TSs have a HC=N–CH_2 bond angle of 177.7 and 114.9°, and only one imaginary frequency of 274i and 325i cm^{-1}, respectively. Therefore, these first-order saddle points are real transition states. The vibrational mode of the neutral TS is associated with the reaction coordinate that involves major motion of the nitrogen atom (in-plane lateral shift), whereas the vibrational mode of the protonated TS is associated with the reaction coordinate that involves major motion of the hydrogen atoms HC=N and NH. Therefore, the protonation has two effects: the first is evident and it is to alter the geometry of the transition state and to significantly decrease its energy for the isomerization process, whereas the second effect is less certain, but most likely makes the *Z* isomer thermodynamically more stable than the *E* isomer. This could also explain why the isomerization is not observed with only a small, catalytic amount of acid. Finally, it should be pointed out that whereas the DFT calculations apparently reproduce the ground-state structures very well, the energies of the transition states are presumably overemphasized.

Rhenium Complexes of 1

The reaction of $Re(CO)_5Cl$ with ***E*-1** in refluxing toluene, under an Ar atmosphere, produces the corresponding complex (***E*-1**)$Re(CO)_3Cl$ (**Re-*E*-1**). When carrying out the same reaction in the presence of an approximately half molar quantity of CF_3COOH, we obtained a mixture of **Re-*E*-1** and (***Z*-1**)$Re(CO)_3Cl$, hereafter called **Re-*Z*-1**. The latter compound was obtained only in small amounts. Remarkably, **Re-*E*-1** and **Re-*Z*-1** have different solubilities in benzene, and can be separated by a simple extraction. The two rhenium-imino derivatives **Re-*E*-1** and **Re-*Z*-1** have been fully characterized with several spectroscopic techniques. In particular, the ^{1}H NMR spectrum of **Re-*E*-1** in CD_2Cl_2 shows three resonances at δ = 9.63, 6.23, and 5.60 ppm, assigned to H(11) and to the two diastereotopic CH_2 protons H(12a) and H(12b), respectively, whereas in the case of **Re-*Z*-1** the corresponding signals are observed at δ = 9.99, 5.12, and 4.76 ppm.

More interestingly, the NOESY experiment on **Re-*E*-1** reveals the presence of a dipolar interaction between H(11) and the two H(12) protons, which is absent in the case of **Re-*Z*-1** (see Supporting Information). Determination of the X-ray structures of the two isomers **Re-*E*-1** and **Re-*Z*-1** confirms the retention of the ligand conformation on coordination to the metal center (Figure 3). The isomerization does not take place after the metal complex formation, since the NMR spectra of **Re-*E*-1** and **Re-*Z*-1** in CD_2Cl_2 solutions before and after the addition of a molar amount of CF_3COOH are identical, most likely because the coordination of the metal does not allow the protonation of the ligand, which then freezes the isomerization process.

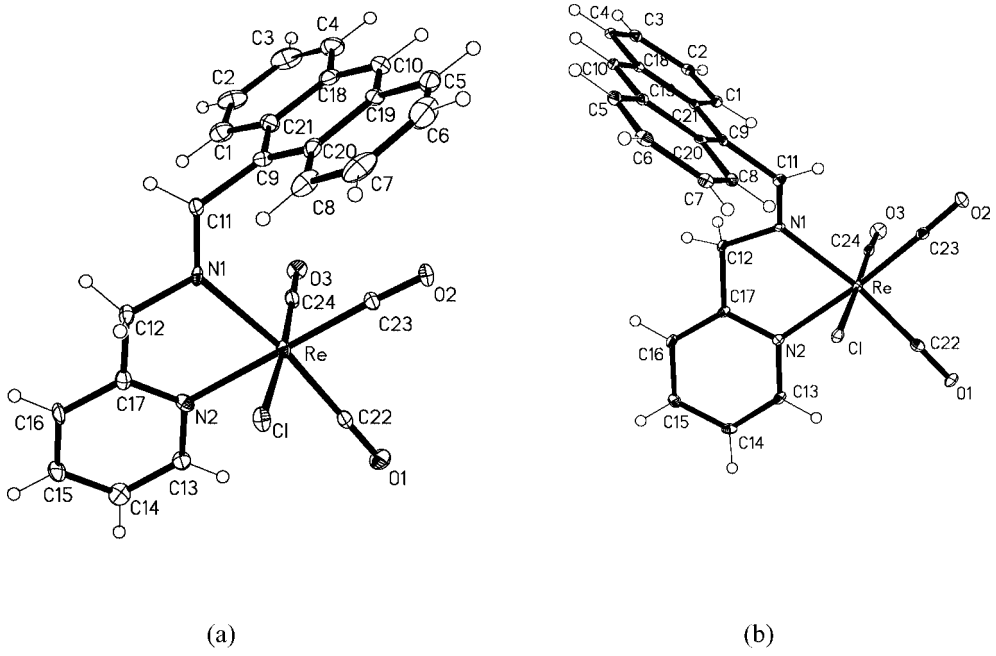

Figure 3. Molecular structures of **Re-*E*-1** (a) and **Re-*Z*-1** (b), showing the adopted labeling scheme, with displacement ellipsoids drawn at the 20% probability. A solvated benzene molecule in **Re-*Z*-1** is not shown for the sake of clarity.

Crystal Structure Analysis

The structures of **Re-*E*-1** and **Re-*Z*-1** isomers are illustrated in Figure 3 and the crystallographic data are given in Table 5. **Re-*E*-1** is arranged in the $P2_1$ chiral space group, while **Re-*Z*-1** is arranged in the centrosymmetric $P\bar{1}$ space group. The *E* isomer was therefore obtained chirally pure, while the *Z* isomer is a racemate of the two possible enantiomers. Compound **Re-*Z*-1** crystallizes with one benzene molecule of solvation.

The *E*/*Z* isomerization of the N(1)–C(11) double bond causes significant rearrangements of the overall shape and of the crystal packing of the two complexes. The selected geometric parameters for the two isomers, and the differences and significances with respect to esd's, are reported in Table 3. The larger differences between the two isomers (Δ values larger than 8) are due to the location and the orientation of the anthracene moiety with respect to the metal core of the complex. Also the pyridine group orientation, defined by the Cl–Re–N(2)–C(17) torsion angle, with Δ = 16.5, is rather different in the two isomers. Conversely, the planarity of the anthracene and of the pyridine groups are similar in the two isomers: 0.035(6) and 0.003(5) Å in **Re-*E*-1** and 0,020(3) and 0.003(2) Å in the **Re-*Z*-1** isomer, respectively. As a result of the above mentioned differences, the anthracene group in **Re-*E*-1** is bent towards the C(23)–O(2) and C(23)–O(4) carbonyl groups, the resulting contact distances being rather short (reported with respect to anthracene center of mass, A_{CM} in Table 3), while in **Re-*Z*-1** the anthracene group is located in the external part of the complex, far away from the metal core and the carbonyl groups. The C(11)–H(11) bond shows an opposite behavior, pointing towards carbonyl groups in **Re-*Z*-1** and towards the anthracene moiety of the adjacent molecule in **Re-*E*-1**. This opposite behavior has a dramatic effect on the crystal packing features of the two isomers. In fact, in **Re-*Z*-1** the crystal packing (see Figure 4, b) is clearly driven by the π-π stacking between parallel anthracene moieties, as indicated by the similar distances observed between the anthracene centers of mass (3.694 Å) and between planes containing adjacent anthracene moieties (3.743 Å). On the contrary, in **Re-*E*-1** the anthracene groups once again lie on parallel planes, with a distances between planes of 3.422 Å, much smaller than the distances between the centers of mass (7.823 Å), thus avoiding the π-π stacking.

In **Re-*E*-1** the anthracene moiety is too close to the metal center to allow the π-π stacking observed in **Re-*Z*-1** and the molecules are helicoidally packed, obeying to the 2_1 screw axis. Finally, CH···OC and CH···Cl interactions are also present.

The *E*/*Z* isomerization also affects the coordination geometry of the Re atom, as indicated by the Δ values highlighted in bold character in Table 3. The differences mostly occur with the Cl ligand (Δ values larger than 2 esd.). Smaller differences, close to the detection limit ($1 < \Delta < 2$ in Table 3) involve the C(24)–O(3) distance and the N(2) atom of the pyridine ligand.

Table 3. Selected geometric parameters for **Re-*E*-1** and **Re-*Z*-1** (distances in Å and angles in °) and relevance of difference with respect to esd's (Δ), calculated as Δ = {esd.[value(**Re-*E*-1**), value(**Re-*Z*-1**)]}/{esd.[value(**Re-*E*-1**)] + esd.[value(**Re-*Z*-1**)]}. Values differing by a significant value (Δ > 1) are highlighted in **bold**.

	Re-*E*-1	**Re-*Z*-1**	Δ
Distances			
Re(1)–Cl(1)	2.474(2)	2.483(1)	**2.1**
Re(1)–N(1)	2.203(8)	2.173(3)	**1.9**
Re(1)–N(2)	2.178(8)	2.184(3)	0.4
Re(1)–C(22)	1.914(10)	1.925(4)	0.6
Re(1)–C(23)	1.945(9)	1.926(4)	1.0
Re(1)–C(24)	1.898(11)	1.912(5)	0.6
O(1)–C(22)	1.149(12)	1.155(5)	0.2
O(2)–C(23)	1.136(11)	1.152(5)	0.7
O(3)–C(24)	1.173(13)	1.146(5)	**1.1**
N(1)–C(15)	1.262(12)	1.287(5)	1.0
N(1)–C(16)	1.472(11)	1.472(5)	0.0
N(2)–C(17)	1.341(12)	1.351(5)	0.4
N(2)–C(21)	1.372(12)	1.352(5)	0.8
C(1)–C(15)	1.494(14)	1.478(5)	0.6
C(16)–C(17)	1.493(13)	1.505(5)	0.5
H(15)–O(2)	5.24(2)	3.15(1)	**49.3**
$A_{CM}^{(*)}$–Re	4.39(1)	5.932(3)	**83.9**
$A_{CM}^{(*)}$–O(2)	3.59(1)	6.522(5)	**138.2**
$A_{CM}^{(*)}$–O(3)	4.36(1)	7.164(5)	**132.2**
$A_{CM}^{(*)}$–C(23)	3.58(1)	6.149(5)	**121.1**
$A_{CM}^{(*)}$–C(24)	4.11(1)	6.531(5)	**114.1**
Angles			
C(22)–Re–Cl	95.2(3)	94.9(1)	0.5
C(23)–Re–Cl	93.6(3)	91.7(1)	**3.4**
C(24)–Re–Cl	176.1(3)	178.2(1)	**3.7**
N(1)–Re–Cl	83.7(2)	83.4(1)	0.7
N(2)–Re–Cl	80.9(2)	82.8(1)	**4.4**
C(24)–Re–N(2)	96.4(4)	96.6(1)	0.3
C(22)–Re–N(2)	96.0(3)	96.9(1)	**1.6**
C(23)–Re–N(2)	174.1(3)	171.6(1)	0.7
C(24)–Re–N(1)	92.9(4)	94.8(1)	**2.7**
C(22)–Re–N(1)	171.7(3)	172.9(1)	0.4
C(23)–Re–N(1)	101.6(4)	97.2(1)	**2.1**
N(2)–Re(1)–N(1)	75.6(3)	76.0(1)	0.7
C(24)–Re–C(22)	87.9(4)	86.9(2)	**1.2**
C(24)–Re–C(23)	88.9(4)	88.7(2)	0.2
C(22)–Re–C(23)	86.7(4)	89.8(2)	**3.7**
C(15)–N(1)–Re	131.4(7)	125.9(3)	**1.3**
C(16)–N(1)–Re	111.9(6)	114.7(2)	0.7
C(17)–N(2)–Re	116.5(6)	116.9(3)	0.1
C(21)–N(2)–Re	125.0(7)	125.1(3)	0.0
O(1)–C(22)–Re	177.9(10)	176.1(4)	0.5
O(2)–C(23)–Re	177.1(8)	178.1(4)	0.2
O(3)–C(24)–Re	179.9(11)	176.7(4)	0.9
N(1)–C(15)–C(1)	124.2(9)	126.5(4)	0.5
N(2)–C(17)–C(16)	117.7(8)	117.4(3)	0.1
N(1)–C(16)–C(17)	111.5(8)	110.9(3)	0.1
C(11)–H(11)–O(2)	16(1)	137(1)	**24.4**
C(23)–O(2)–$A_{CM}^{(*)}$	80.1(8)	66.2(4)	**8.2**
C(24)–O(3)–$A_{CM}^{(*)}$	70.0(8)	52.6(4)	**10.3**
Torsion angles			
Cl–Re–N(2)–C(17)	71.2(6)	92.2(3)	**16.5**
Cl–Re–N(1)–C(11)	123(1)	74.3(5)	**23.2**
Re–N(1)–C(11)–C(9)	–6(2)	–175(1)	**39.8**
C(20)–C(9)–C(11)–N(1)	–84(1)	115.7(5)	**94.1**

$A_{CM}^{(*)}$ = center of mass of anthracene moiety

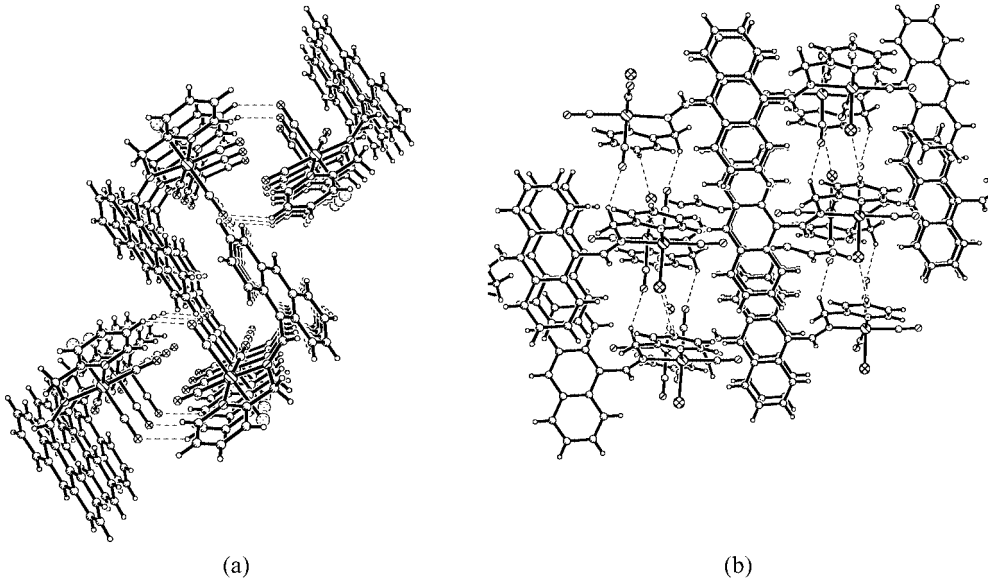

Figure 4. The crystal packing of **Re-*E*-1** (a) and **Re-*Z*-1** (b).

Electronic Absorption and Emission Spectra

The electronic absorption spectrum of ***E*-1** in CH_3CN solution shows an intense absorption peak at 251 nm (ε = 64800 M^{-1}) and three bands at 351, 369, and 387 nm, which probably correspond to the $\pi\rightarrow\pi^*$ and $n\rightarrow\pi^*$ transitions. Excitation at 370 nm in CH_3CN produces an intense emission peak at 440 nm. These absorption and emission peaks are very similar to those of pure anthracene.[34] Rhenium complexes **Re-*E*-1** and **Re-*Z*-1** have identical absorption (bands at 354, 371, and 389 nm) and emission spectra, which in turn are very similar to that of the free ligand ***E*-1**. However, **Re-*E*-1** and **Re-*Z*-1** show a weaker emission centered at 441 nm (Figure 5). We did not observe a metal-centered MLCT emission band. $Re(bpy)(CO)_3Cl$ and analogous imino derivatives[8,12,35] usually have MLCT absorptions in the range 340–430 nm. Time-Dependent DFT calculations (TDDFT) help to understand these data. The geometries of ***E*-1**, **Re-*E*-1**, and **Re-*Z*-1** were optimized in the singlet ground state in the gas phase. The HOMO and LUMO of ***E*-1** are mostly localized on the anthracene unit, only slightly involving the C=N double bond. The spectroscopic properties were calculated employing the combined TDDFT/CPCM computational approach, which is currently considered to be the most appropriate method for the treatment of the solvent effects on the excited-state energies of transition-metal complexes.[36,37] A number of singlet excited states of ***E*-1**, **Re-*E*-1**, and **Re-*Z*-1** in acetonitrile were calculated and are reported in Table 4. The absorption of ***E*-1** with the highest oscillator strength (393 nm) is mainly from a HOMO→LUMO transition. In the case of **Re-*E*-1** and **Re-*Z*-1**, the absorptions calculated at 420 and 424 nm are still largely HOMO→LUMO transitions, and therefore labeled as ligand-centered transitions, with a modest contribution from the metal ion. This supports the absence of charge transfer states observed in the absorption and emission spectra of the free ligands and metal complexes. Furthermore, there is a very small effect of the rhenium atom on the fluorescence lifetime. In fact, the average lifetime is 11.5 ns for the ligand and 11.3 ns for the complexes.

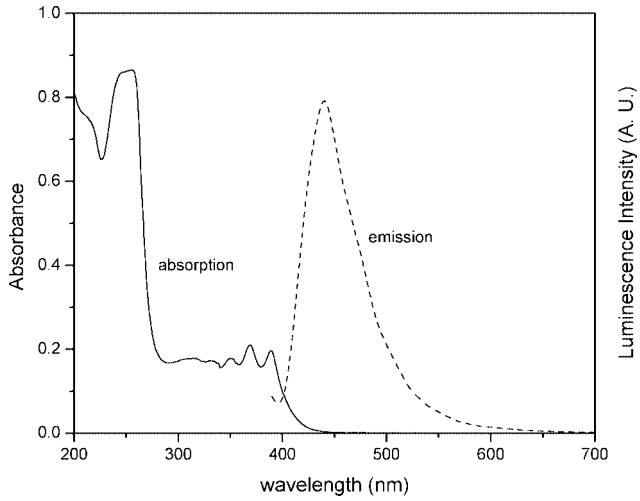

Figure 5. Absorption and emission spectra (excitation at 370 nm) of **Re-*E*-1** in CH_3CN.

Table 4. Energies (in nm) and oscillator strengths (*f*) of the first calculated singlet excited states for ***E*-1**, **Re-*E*-1**, and **Re-*Z*-1** in acetonitrile.

***E*-1**		**Re-*E*-1**		**Re-*Z*-1**	
f	*E* [nm]	*f*	*E* [nm]	*f*	*E* [nm]
		0.14	420	0.21	424
0.089	393	0.03	374	0.002	374
0.001	335	0.04	368	0.02	366
0.003	319	0.02	354	0.001	357
0.001	298	0.03	343	0.001	334
0.001	293	0.001	336	0.001	333

Electrochemistry

The electrochemical behavior of the rhenium complexes **Re-*E*-1** and **Re-*Z*-1** has been investigated by cyclic voltammetry (CV) and square wave voltammetry (SWV) in CH_2Cl_2 solutions using glassy carbon as a working electrode, under an Ar atmosphere. The CV response of **Re-*E*-1**, identical to that of **Re-*Z*-1**, exhibits a 1e chemically irreversible reduction at E_p = –1.89 V vs. Fc/Fc^+, and a multi-electron chemically irreversible oxidation at E_p = +1.11 V vs. Fc/Fc^+. Our attempts to slow down the chemical complications by lowering the temperature were unsuccessful. CV performed as low as –80 °C and at a scan rate between 0.05 and 5 V/s did not freeze the homogeneous chemical reactions and the redox processes remained chemically irreversible.

Experimental Section

(*E*)-*N*-(Methyl-2-pyridyl)antracen-9-carboxaldimine (*E*-1): Anthracene-9-carboxaldehyde (1.00 g, 4.85 mmol) was dissolved in absolute ethanol (250 mL) and the solution was degassed for 10 min under argon. 2-(Aminomethyl)pyridine (0.524 g, 4.85 mmol) was added and the solution was refluxed for 1.5 h. After evaporation of the solvent, the yellow solid was washed with hexane (20–25 mL) and recrystallized from ethanol (yield 75%, 1.078 g). ^{1}H NMR [400 MHz, $(CD_3)_2CO$, 25 °C]: δ = 9.75 (s, 1 H), 8.75 [d, $^3J_{H,H}$ = 7.7 Hz, 2 H], 8.65 (s, 1 H), 8.61 (d, $^3J_{H,H}$ = 4.2 Hz, 1 H), 8.11 (d, $^3J_{H,H}$ = 8.4 Hz, 2 H), 7.78 (t, $^3J_{H,H}$ = 7.7 Hz, 1 H), 7.60 (d, $^3J_{H,H}$ = 7.9 Hz, 1 H), 7.53 (m, 4 H), 7.28 (t, $^3J_{H,H}$ = 6.4 Hz, 1 H), 5.25 (s, 2 H) ppm. ^{1}H NMR (400 MHz, CD_2Cl_2, 25 °C): δ = 9.63 (t, $^3J_{H,H}$ = 1.3 Hz, 1 H, 11-H), 8.61 (m, 2 H, 1-H and 8-H), 8.59 (m, 1 H, 13-H), 8.53 (s, 1 H, 10-H), 8.06 (dd, $^3J_{H,H}$ = 7.9 and 1.9 Hz, 2 H, 4-H and 5-H), 7.72 (t, $^3J_{H,H}$ = 7.7 and 1.9 Hz, 1 H, 15-H), 7.52 (m, 5 H, 16-H, 2-H, 3-H, 6-H, 7-H), 7.23 (dd, $^3J_{H,H}$ = 5.0 and 1.1 Hz, 1 H, 14-H), 5.23 (d, $^3J_{H,H}$ = 1.3 Hz, 2 H, 12-H) ppm. ^{13}C NMR [100 MHz, $(CD_3)_2CO$, 25 °C]: δ = 162.34, 159.69, 149.51, 136.72, 131.60, 130.27, 129.59, 128.99, 128.56, 126.80, 125.54, 125.40, 122.54, 122.24, 68.15 ppm. ^{13}C NMR (100 MHz, CD_2Cl_2, 25 °C): δ = 162.46, 159.54, 149.70, 136.92, 131.63, 130.37, 129.77, 129.11, 128.52, 126.98, 125.62, 125.27, 122.75, 122.39, 68.68 ppm. Electronic spectrum in CH_3CN: absorption, λ_{max} = 251, 351, 369, 387 nm, emission, λ_{max} = 440 nm.

(*Z*)-*N*-(2-Pyridylmethyl)antracen-9-carboxaldimine (*Z*-1): The *Z* isomer was obtained from the irradiation for 3 h at 365 nm, 50 W, of a CH_2Cl_2 solution of the *E* isomer containing an equimolar amount of CF_3COOH. The conversion occured without any side reaction. ^{1}H NMR (400 MHz, CD_2Cl_2, 25 °C) of the protonated species: δ = 11.40 (s, 1 H), 9.02 (dd, $^3J_{H,H}$ = 9.0 and 0.8 Hz, 2 H), 8.82 (s, 1 H), 8.80 (dd, $^3J_{H,H}$ = 5.9 and 1.3 Hz, 1 H), 8.58 (t, $^3J_{H,H}$ = 7.9 Hz, 1 H), 8.19 (d, $^3J_{H,H}$ = 7.9 Hz, 1 H) 8.12 (d, $^3J_{H,H}$ = 8.4 Hz, 2 H), 8.06 (t, $^3J_{H,H}$ = 5.9 Hz, 1 H), 7.75 (dd, $^3J_{H,H}$ = 9.0 and 1.5 Hz, 2 H), 7.60 (dd, $^3J_{H,H}$ = 8.6 and 1.0 Hz, 2 H), 4.80 (s, 2 H) ppm. ^{13}C NMR (100 MHz, CD_2Cl_2, 25 °C): δ = 195.24, 147.77, 146.13, 143.11, 137.68, 133.15, 131.10, 130.15, 129.85, 129.68, 128.13, 126.02, 123.29, 40.94 ppm.

Re(*E*-1)(CO)$_3$Cl (Re-*E*-1): $Re(CO)_5Cl$ (300 mg) was refluxed in toluene (50 mL) for 2 h with a 10% excess of ***E*-1** (270 mg) under argon. The solution was then cooled before the yellow product was filtered and washed with toluene and hexane. Finally, the solid was dried in vacuo (yield 78%, 390 mg). ^{1}H NMR [400 MHz, $(CD_3)_2CO$, 25 °C]: δ = 9.96 (s, 1 H), 8.87 (d, $^3J_{H,H}$ = 5.4 Hz, 1 H), 8.77 (s, 1 H), 8.15 (m, 4 H), 98.04 (d, $^3J_{H,H}$ = 8.5 Hz, 1 H), 7.91 (d, $^3J_{H,H}$ = 7.8 Hz, 1 H), 7.53 (m, 5 H), 6.29 (d, $^3J_{H,H}$ = 18.3 Hz, 1 H), 6.06 (d, $^3J_{H,H}$ = 18.6 Hz, 1 H) ppm. ^{1}H NMR (400 MHz, CD_2Cl_2, 25 °C): δ = 9.63 (s, 1 H), 8.82 (d, $^3J_{H,H}$ = 5.3 Hz, 1 H), 8.70 (s, 1 H), 8.13 (m, 2 H), 8.06 (d, $^3J_{H,H}$ = 8.5 Hz, 1 H), 8.00 (t, $^3J_{H,H}$ = 7.9 Hz, 1 H), 7.81 (m, 1 H), 7.65 (m, 2 H), 7.56 (m, 3 H), 7.38 (t, $^3J_{H,H}$ = 6.5 Hz, 1 H), 6.23 (d, $^3J_{H,H}$ = 18.2 Hz, 1 H), 5.60 (d, $^3J_{H,H}$ = 18.2 Hz, 1 H) ppm. ^{13}C NMR [100 MHz, $(CD_3)_2CO$, 25 °C]: δ = 198.11, 194.40, 191.62, 175.53, 160.38, 152.34, 139.66, 131.43, 131.21, 129.87, 128.84, 128.75, 128.24, 126.74, 126.60, 125.90, 125.78, 125.34, 124.57, 122.14, 69.12 ppm. IR (powder-ATR): $\tilde{\nu}$ = 2025, 1922, 1897 cm^{-1}. ^{13}C NMR (100 MHz, CD_2Cl_2, 25 °C): δ = 198.11, 194.40, 191.62, 174.71, 163.26, 159.13, 152.95, 139.57, 131.50, 131.29, 130.48, 129.41, 129.16, 128.31, 127.54, 127.29, 126.38, 125.55, 124.88, 124.75, 121.89, 69.78 ppm. Electronic spectrum in CH_3CN: absorption, λ_{max} = 255, 317, 335, 354, 372, 391 nm, emission, λ_{max} = 440 nm.

Re(*Z*-1)(CO)$_3$Cl (Re-*Z*-1): The complex was obtained as a side product during a modified synthesis of **Re-*E*-1**. $Re(CO)_5Cl$ (200 mg) was stirred in toluene (50 mL) with a 10% excess of ***E*-1** (180 mg) under argon. CF_3COOH (30 μL) was added, and the solution was refluxed for 4 h. After cooling at room temperature, a yellow precipitate of **Re-*E*-1** and a red solution containing a mixture of **Re-*E*-1** and **Re-*Z*-1** were obtained. The solution was filtered, and the solvent evaporated. The solid was treated with benzene, which only dissolved **Re-*Z*-1**. Finally, the solvent was evaporated and the solid dried in vacuo (yield 15%, 50 mg). ^{1}H NMR (400 MHz, CD_2Cl_2, 25 °C): δ = 9.99 (t, $^3J_{H,H}$ = 2.3 Hz, 1 H), 8.89 (d, $^3J_{H,H}$ = 5.3 Hz, 1 H), 8.72 (s, 1 H), 8.22 (d, $^3J_{H,H}$ = 8.4 Hz, 1 H), 8.16 (m, 2 H), 7.83 (d, $^3J_{H,H}$ = 8.4 Hz, 1 H), 7.75 (t, $^3J_{H,H}$ = 7.9 and 1.6 Hz, 1 H), 7.61 (m, 4 H), 7.33 (t, $^3J_{H,H}$ = 6.7 Hz, 1 H), 7.01 (d, $^3J_{H,H}$ = 7.9 Hz, 1 H), 5.12 (dd, $^3J_{H,H}$ = 19.0 and 2.5 Hz, 1 H), 4.76 (dd, $^3J_{H,H}$ = 19.0 and 2.5 Hz, 1 H) ppm. IR (powder-ATR): $\tilde{\nu}$ = 2024, 1921, 1896 cm^{-1}. Electronic spectrum in CH_3CN: absorption, λ_{max} = 255, 303, 335, 354, 372, 391 nm, emission, λ_{max} = 440 nm.

Physical Methods: The NMR spectra were recorded with a JEOL EX 400 spectrometer (B_0 = 9.8 T) with chemical shifts referenced to residual protons in the solvent (CD_2Cl_2). COSY and NOESY experiments were acquired using standard procedures. IR spectra were recorded as powder-ATR using a Thermo-Nicolet 670 FT-IR spectrophotometer with a resolution of 1 cm^{-1} and an accumulation of 64 scans. Absorption spectra were measured at room temperature, in CH_2Cl_2, using a Hitachi U-3210 double-beam spectrophotometer, and emission spectra were measured with a SLM 4800 spectrofluorimeter. Luminescence lifetimes were performed under magic-angle polarization conditions by time-correlated single-photon counting using excitation with picosecond pulses of 370 nm light at a repetition rate of 500 kHz generated by a Ti:Sapphire laser system (Verdi V10, Mira 900, and pulse picker from Coherent, Inc., Santa Clara, CA. Second harmonic generation was provided by a 5–050 system from Inrad, Northvale, NJ). The sample was maintained at 20 °C in an automated sample chamber (FLASC 1000 from Quantum Northwest, Spokane, WA). The emission was collected using a bandpass of 20 nm. The data were collected into 2048 channels (0.25 ns/channel) to 40,000 counts in the peak channel. Because the excitation pulse is essentially a delta function at this time resolution, the decays were fitted directly without reconvolution as sums of exponentials using Origin 7 (Northampton, MA 01060, USA).

X-ray Structure Determinations: Single crystal diffraction data were collected at 100 K, using an Oxford Cryostream low temperature

device, on an Oxford Xcalibur CCD area detector diffractometer, using graphite monochromatic Mo-K_α (λ = 0.71069 Å) radiation. Data reduction and absorption corrections were performed using CrysAlis RED 1.171.26 (Oxford Diffraction). The structure was solved by direct methods using SIR2004[38] and refined by full-matrix least-squares using SHELX-97.[39] All hydrogen atoms were located in the electron density map and then refined using isotropic displacement parameters.

The Crystallographic Information File (CIF) has been deposited with deposition number CCDC-298650 for the **Re-*E*-1** structure and CCDC-298651 for the **Re-*Z*-1** structure. These data can be obtained free of charge from The Cambridge Crystallographic Data Centre via www.ccdc.cam.ac.uk/data_request/cif. Details of data collections and refinements are given in Table 5.

Table 5. Crystallographic data for **Re-*E*-1** and **Re-*Z*-1** isomers.

	Re-*E*-1	**Re-*Z*-1**
Empirical formula	$C_{24}H_{16}ClN_2O_3Re$	$C_{24}H_{16}ClN_2O_3Re$
Formula mass [g/mol]	602.04	602.04
Temperature [K]	123 (2)	100 (2)
Wavelength [Å]	0.71073	0.71073
Crystal system	$P2_1$	$P\bar{1}$
Space group	monoclinic	triclinic
Unit cell dimensions	a = 11.222(1)	a = 8.834(1)
(edges in Å and angles in °)	b = 7.712(1)	b = 11.494(1)
	c = 12.761(1)	c = 12.327(1)
	β = 96.564(5)°	α = 80.55(1)
		β = 80.32(1)
		γ = 74.42(1)
Volume [Å^3]	1097.1(1)	1179.0(2)
Z	2	2
Density (calculated) [mg/m^3]	1.822	1.693
Absorption coefficient [mm^{-1}]	5.688	5.292
F(000)	580	578
Crystal size [mm]	0.35×0.15×0.09	0.11×0.25×0.20
Theta range for data collection [°]	1.61 to 27.50	4.40 to 20.81
Index ranges	$-14 \le h \le 14$	$-8 \le h \le 8$
	$-10 \le k \le 10$	$-11 \le k \le 11$
	$-16 \le l \le 16$	$-12 \le l \le 12$
Reflections collected	15981	5316
Independent reflections	5023	2452
	[R(int) = 0.0851]	[R(int) = 0.0181]
Completeness to θ = 20.81°	99.9%	99.0%
Refinement method	Full-matrix least-squares on F^2	Full-matrix least-squares on F^2
Data/restraints/parameters	5023/1/280	2452/0/307
Goodness-of-fit on F^2	1.005	1.066
Final R indices [$I > 2\sigma(I)$]	R_1 = 0.0488,	R_1 = 0.0194,
	wR_2 = 0.1135	wR_2 = 0.0396
R indices (all data)	R_1 = 0.0637,	R_1 = 0.0225,
	wR_2 = 0.1215	wR_2 = 0.0407
Largest diff. peak and hole [e/Å^3]	2.836 and –1.748	1.021 and –0.365

Electrochemistry: Dichloromethane was distilled over calcium hydride just before use. Tetrabutylammonium hexafluorophosphate (Bu_4NPF_6) was obtained from a metathesis reaction between KPF_6 (Fluka) and tetrabutylammonium iodide (Aldrich), recrystallized three times from 95% ethanol and dried in a vacuum oven at 110 °C overnight. The electrochemistry was performed in a three-electrode cell using a potentiostat AMEL 7050 and an EG&G PAR 273 electrochemical analyzer, both connected to a PC. The reference electrode was a 3 M KCl Calomel Electrode, the auxiliary electrode a platinum wire, and the working electrode a glassy carbon (GC). Positive feedback *iR* compensation was applied routinely. All measurements were carried out under Ar in anhydrous deoxygenated solvents. We used ferrocene (Fc) as the internal standard, and potentials are reported against the Fc(0/+1) redox couple, which under our conditions is $E°$(0/+1) = 0.595 V.

DFT Calculations: The DFT method with Becke's[40] three-parameter hybrid functional and Lee–Yang–Parr's[41] gradient corrected correlation functional was used. The calculations have been made with the Gaussian 03 (G03)[28] and Jaguar[24] programs. The Stuttgart–Dresden (SDD) ECP[42] was used for the Re atom and the 6-311++G** basis set for all other atoms. Calculations of the absolute magnetic shielding σ were performed at the B3LYP/6-311++G** level using either G03 or Jaguar. The σ absolute values were converted into proton chemical shifts δ, relative to the magnetic shielding of tetramethylsilane computed with the same basis set (31.9793, H and 184.1441, C for G03; 31.9821, H and 184.0820, C for Jaguar). The nature of transition states was confirmed by performing a harmonic vibrational frequencies calculation and a normal-mode analysis. Vibrational frequencies and Gibbs free energy calculations were performed at 298.15 K and 1 atm. Time-dependent density functional theory[43,44] (TDDFT) combined with the conductor-like polarizable continuum model[45–47] (CPCM) method with acetonitrile as solvent has been used to calculate the excited-state energies by means of G03.

Supporting Information (see also the footnote on the first page of this article): ^{1}H, ^{1}H-^{1}H COSY and ^{1}H-^{1}H NOESY NMR spectra of ***E*-1**, **Re-*E*-1**, and **Re-*Z*-1** in CD_2Cl_2, and the ^{1}H NMR spectra of **1** before, after, and during its *E* to *Z* isomerization by means of CF_3COOH in CD_2Cl_2.

Acknowledgments

We gratefully acknowledge the Italian MURST (PRIN 2005), Regione Piemonte, and the Department of Energy (E.R., grant # DE-FG02-01ER45869). J.B.A.R. gratefully acknowledges support by NSF MCB-0517644 and by NIH COBRE RR-15583. We thank Centre of Excellence for Molecular Imaging (Torino), and Ayesha Sharmin, University of Montana for IR powder-ATR measurements.

[1] W. P. Griffith, in: *Comprehensive Coordination Chemistry* (Eds.: G. Wilkinson, J. A. McCleverty), Pergamon, Oxford, **1987**, p. 519.
[2] M. Schröder, T. A. Stephenson, in: *Comprehensive Coordination Chemistry* (Eds.: G. Wilkinson, J. A. McCleverty), Pergamon, Oxford, **1987**, p. 277.
[3] V. Balzani, F. Scandola, *Supramolecular Photochemistry*, Ellis-Horwood, Chichester, UK, **1991**.
[4] K. Kalyansundaram, *Photochemistry of Polypyridine and Porphyrin Complexes*, Academic Press, New York, **1992**.
[5] J. Hawecker, J. M. Lehn, R. Ziessel, *J. Chem. Soc., Chem. Commun.* **1984**, 328.
[6] B. P. Sullivan, T. J. Meyer, *J. Chem. Soc., Chem. Commun.* **1984**, 1244.
[7] D. M. Dattelbaum, K. M. Omberg, P. J. Hay, N. L. Gebhart, R. L. Martin, J. R. Schoonover, T. J. Meyer, *J. Phys. Chem. A* **2004**, *108*, 3527–3536.
[8] N. M. Shavaleev, Z. R. Bell, G. Accorsi, M. D. Ward, *Inorg. Chim. Acta* **2003**, *351*, 159–166.
[9] H. Hartmann, T. Scheiring, J. Fiedler, W. Kaim, *J. Organomet. Chem.* **2000**, *604*, 267–272.
[10] S. Frantz, J. Fiedler, I. Hartenbach, T. Schleid, W. Kaim, *J. Organomet. Chem.* **2004**, *689*, 3031–3039.
[11] S. Frantz, M. Weber, T. Scheiring, J. Fiedler, C. Duboc, W. Kaim, *Inorg. Chim. Acta* **2004**, *357*, 2905–2914.
[12] R. N. Dominey, B. Hauser, J. Hubbard, J. Dunham, *Inorg. Chem.* **1991**, *30*, 4754–4758.

[13] W. W. Wang, B. Spingler, R. Alberto, *Inorg. Chim. Acta* **2003**, *355*, 386–393.
[14] J. E. Johnson, N. M. Morales, A. M. Gorczyca, D. D. Dolliver, M. A. McAllister, *J. Org. Chem.* **2001**, *66*, 7979.
[15] K. D. Karlin, Z. Tyeklar, *Bioinorganic Chemistry of Copper*, Chapman and Hall, New York, **1993**.
[16] F. Fache, E. Schulz, M. L. Tommasino, M. Lemaire, *Chem. Rev.* **2000**, *100*, 2159–2231.
[17] J. Royer, M. Bonin, L. Micouin, *Chem. Rev.* **2004**, *104*, 2311–2352.
[18] J. M. Villegas, S. R. Stoyanov, D. P. Rillema, *Inorg. Chem.* **2002**, *41*, 6688–6694.
[19] S. R. Stoyanov, J. M. Villegas, D. P. Rillema, *Inorg. Chem.* **2002**, *41*, 2941–2945.
[20] F. Fischer, Y. Frei, *J. Chem. Phys.* **1957**, *27*, 808.
[21] G. Wettermark, L. Dogliotti, *J. Chem. Phys.* **1964**, *40*, 1486.
[22] M. Maruyama, Y. Kaizu, *Inorg. Chim. Acta* **1996**, *247*, 155.
[23] A. K. Ghosh, K. K. Kamar, P. Paul, S. M. Peng, G. H. Lee, S. Goswami, *Inorg. Chem.* **2002**, *41*, 6343–6350.
[24] Jaguar, Version 6.5, Schrodinger, LLC, New York, NY, **2005**.
[25] J. Bjørgo, D. R. Boyd, C. G. Watson, W. B. Jennings, *J. Chem. Soc., Perkin Trans. 2* **1974**, 757–762.
[26] H. B. Bürgi, J. D. Dunitz, *J. Chem. Soc. C* **1969**, 472–473.
[27] D. G. Musaev, K. Hirao, *J. Phys. Chem. A* **2003**, *107*, 1563–1573.
[28] M. J. Frisch, G. W. Trucks, H. B. Schlegel, G. E. Scuseria, M. A. Robb, J. R. Cheeseman, J. A. Montgomery Jr, T. Vreven, K. N. Kudin, J. C. Burant, J. M. Millam, S. S. Iyengar, J. Tomasi, V. Barone, B. Mennucci, M. Cossi, G. Scalmani, N. Rega, G. A. Petersson, H. Nakatsuji, M. Hada, M. Ehara, K. Toyota, R. Fukuda, J. Hasegawa, M. Ishida, T. Nakajima, Y. Honda, O. Kitao, H. Nakai, M. Klene, X. Li, J. E. Knox, H. P. Hratchian, J. B. Cross, C. Adamo, J. Jaramillo, R. Gomperts, R. E. Stratmann, O. Yazyev, A. J. Austin, R. Cammi, C. Pomelli, J. Ochterski, P. Y. Ayala, K. Morokuma, G. A. Voth, P. Salvador, J. J. Dannenberg, V. G. Zakrzewski, S. Dapprich, A. D. Daniels, M. C. Strain, O. Farkas, D. K. Malick, A. D. Rabuck, K. Raghavachari, J. B. Forestman, J. V. Ortiz, Q. Cui, A. G. Baboul, S. Clifford, J. Cioslowski, B. B. Stefanov, G. Liu, A. Liashenko, P. Piskorz, I. Komaromi, R. L. Martin, D. J. Fox, T. Keith, M. A. Al-Laham, C. Y. Peng, A. Nanayakkara, M. Challacombe, P. M. W. Gill, B. Johnson, W. Chen, M. W. Wong, C. Gonzales, J. A. Pople, *Gaussian 03*, Version revision C.02, Gaussian Inc., Wallingford CT, **2004**.
[29] T. J. Lang, G. J. Wolber, R. D. Bach, *J. Am. Chem. Soc.* **1981**, *103*, 3275–3282.
[30] R. D. Bach, J. J. W. McDouall, A. L. Owensby, H. B. Schlegel, J. W. Holubka, J. C. Ball, *J. Phys. Org. Chem.* **1991**, *4*, 125–134.
[31] T. Helgaker, M. Jaszunski, K. Ruud, *Chem. Rev.* **1999**, *99*, 293–352.
[32] R. Gobetto, C. Nervi, B. Romanin, L. Salassa, M. Milanesio, G. Croce, *Organometallics* **2003**, *22*, 4012–4019.
[33] M. Kaupp, M. Bühl, V. G. Malkin, *Calculation of NMR and EPR Parameters - Theory and Applications*, Wiley-VCH, Weinheim, **2004**.
[34] B. Valeur, *Molecular Fluorescence: Principles and Applications*, Wiley-VCH, Weinheim, **2002**.
[35] J. V. Caspar, T. J. Meyer, *J. Phys. Chem. A* **1983**, *87*, 952–957.
[36] S. R. Stoyanov, J. M. Villegas, D. P. Rillema, *Inorg. Chem. Commun.* **2004**, *7*, 838–841.
[37] J. M. Villegas, S. R. Stoyanov, W. Huang, D. P. Rillema, *Inorg. Chem.* **2005**, *44*, 2297–2309.
[38] A. Altomare, M. C. Burla, M. Camalli, G. L. Cascarano, C. Giacovazzo, A. Guagliardi, A. G. Moliterni, G. Polidori, R. Spagna, *J. Appl. Crystallogr.* **1999**, *32*, 115–119.
[39] G. M. Sheldrick, *SHELXL-97*, University of Göttingen, Germany, **1997**.
[40] A. D. Becke, *J. Chem. Phys.* **1993**, *98*, 5648–5652.
[41] C. Lee, W. Yang, R. G. Parr, *Phys. Rev. B: Condens. Matter* **1988**, *37*, 785.
[42] D. Andrae, U. Haussermann, M. Dolg, H. Stoll, H. Preuss, *Theor. Chim. Acta* **1990**, *77*, 123–141.
[43] R. E. Stratmann, G. E. Scuseria, M. J. Frisch, *J. Chem. Phys.* **1998**, *109*, 8218–8224.
[44] M. E. Casida, C. Jamorski, K. C. Casida, D. R. Salahub, *J. Chem. Phys.* **1998**, *108*, 4439–4449.
[45] V. Barone, M. Cossi, *J. Phys. Chem. A* **1998**, *102*, 1995–2001.
[46] M. Cossi, V. Barone, *J. Chem. Phys.* **2001**, *115*, 4708–4717.
[47] M. Cossi, N. Rega, G. Scalmani, V. Barone, *J. Comput. Chem.* **2003**, *24*, 669–681.

Received: March 21, 2006
Published Online: May 29, 2006

